PHYSOR 2004 -The Physics of Fuel Cycles and Advanced Nuclear Systems: Global Developments
Chicago, Illinois, April 25-29, 2004, on CD-ROM, American Nuclear Society, Lagrange Park, IL. (2004)

Measurement and calculation of the ^{233}Pa fission cross-section for advanced fuel cycles

F.-J. Hambsch*[1], F. Tovesson[1,2], S.Oberstedt[1], V. Fritsch[1], A. Oberstedt[2], B. Fogelberg[3], E. Ramström[3], G. Vladuca[4], A. Tudora[4] and D. Filipescu[4]

[1]*EC-JRC-Institute for Reference Materials and Measurements (IRMM), B-2440 Geel, Belgium*

[2]*Örebro University, Department of Natural Sciences, SE-70182 Örebro, Sweden*

[3]*Uppsala University, Department of Radiaton Science, SE-61182 Nyköping, Sweden*

[4]*Bucharest University, Faculty of Physics, RO-76900 Bucharest, Romania*

The energy dependence of the neutron-induced fission cross-section of ^{233}Pa has been measured directly for the first time from the fission threshold up to 8.5 MeV. This fission cross-section is a key ingredient in feasibility studies on fast reactors and accelerator driven systems based on the Th-U fuel cycle. The results are at strong variance with the existing evaluations. The new experimental data give lower cross-section values and resolve the question about the threshold energy. Additionally a new theoretical calculation of the reaction cross-section has been performed with the statistical model code STATIS, showing a very good agreement with the experimental data.

KEYWORDS: Nuclear Reactions ^{233}Pa(n,f), E_n = 1.0-8.5 MeV, fission cross-section vs. neutron energy, comparison with model predictions and evaluated files

1. Introduction

Major research efforts are currently carried out around the world in order to investigate a new concept in nuclear power generation: Accelerator Driven Systems (ADS) [1-3]. These facilities, if realized, would combine the safe generation of electrical power with the possibility of reducing the long-lived fission products and minor actinides in the present stockpile of waste from conventional nuclear reactors through transmutation. A very promising approach is to base the subcritical reactor of such a facility on the Th-U fuel cycle, since thorium is readily available in nature and produces low-radiotoxic waste. This has prompted a re-newed interest for the Th-U fuel cycle, and poses new requirements on the availability and quality of nuclear data relevant to this fuel cycle. In addition to advancements in accelerator design, investigations of radiation effects on structural material, and insight in spallation physics, new nuclear reaction data are crucial for the safe realization of this promising concept.

[1] Corresponding author: Tel. + 32 14 571351, FAX + 32 14571376,
E-mail: franz-josef.hambsch@cec.eu.int

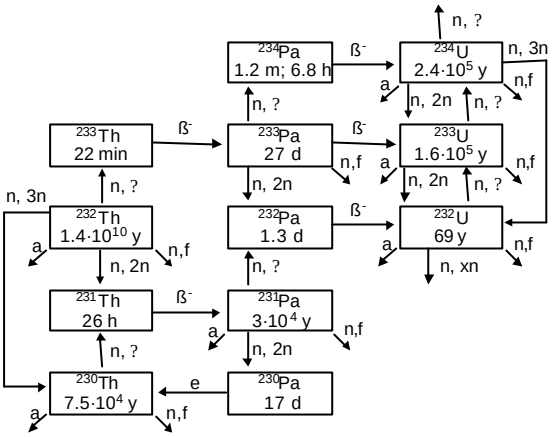

Fig. 1 Schematic view of the thorium fuel cycle. Production and decay modes, as well as half-lives are shown for each isotope. The ^{233}Pa isotope is highlighted.

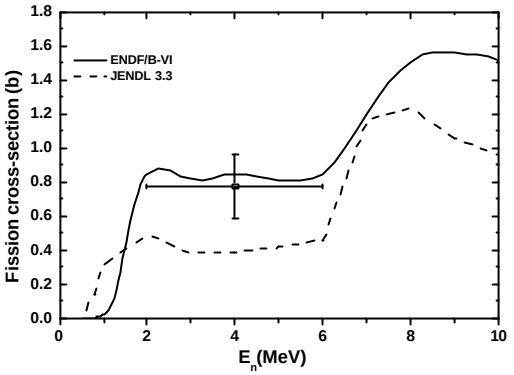

Fig. 2 Fission cross-section evaluations and experimental point from Ref. [6] as a function of incident neutron energy.

Figure 1 shows the most important isotopes in the Th-U fuel cycle and their respective transformation. In a recent IAEA report [4] the priority isotopes in the Th-U fuel cycle have been identified and requirements concerning the different reaction cross-sections formulated.

Of particular interest for reactivity calculations in an ADS is the isotope ^{233}Pa, since it plays a keyrole as an intermediate in the formation of the fuel ^{233}U. Hence, the build-up and decay of ^{233}Pa affect both the breeding of the main fuel ^{233}U and the reactivity behavior of a reactor. The reactions involving ^{233}Pa are responsible for the balance of nuclei. The fairly slow β^- decay of ^{233}Pa into ^{233}U gives also rise to what is known as the protactinium effect [5]: After a reactor stop, the present protactinium will continue to decay into ^{233}U, leading to an increase in reactivity, which even may cause criticality. Hence, the knowledge of the reaction cross-section competing with the natural decay of ^{233}Pa is important.

Until recently no experimental data for the fast neutron induced fission-cross section were available except one measurement dating back to 1967 [6], reporting a value of 775 +/- 190 mb. The measurement was carried out using a reactor neutron spectrum, lacking any energy resolution. With such limited experimental information a theoretical evaluation of the reaction cross-section is very difficult. The available nuclear data libraries, ENDF/B-VI [7] and JENDL-3.3 [8] reflect this situation and differ by approximately a factor of two for the fission cross-section (see Fig. 2).

In view of this new and reliable data were needed. In this paper we present the results from a first direct measurement of the fission cross-section with mono-energetic neutrons and subsequent calculation of the new cross-section dependence in the energy range from 1.0 MeV to 6 MeV.

2. Experiment

The experiments have been performed at the Institute for Reference Materials and Measurements (EC-JRC-IRMM) in Geel, Belgium. The 7 MV Van-de-Graaff (VdG) accelerator facility was used to accelerate proton or deuteron beams onto neutron producing targets. The

covered energy range was from 1.0 to 8.5 MeV incident neutron energy. Three types of targets were used: a titanium-tritium solid target (TiT), a titanium-deuterium solid target (TiD) and a deuterium gas target (D_2-gas). Accordingly, the $T(p,n)^3He$ and $D(d, n)^3He$ reactions were used to produce neutrons with energies of E_n = 1.0 to 3.8 MeV and E_n = 5.0 to 8.5 MeV, respectively. The ^{233}Pa targets were prepared at the Studsvik Neutron Research Laboratory in Nyköping, Sweden. The sample mass of the three samples used was between 0.5 μg and 1.1 μg. More details about the target preparation can be found in Refs. [9, 10].

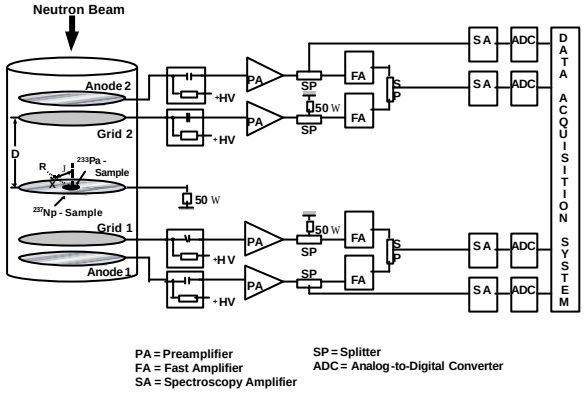

Fig. 3 Schematic view of the experimental set-up.

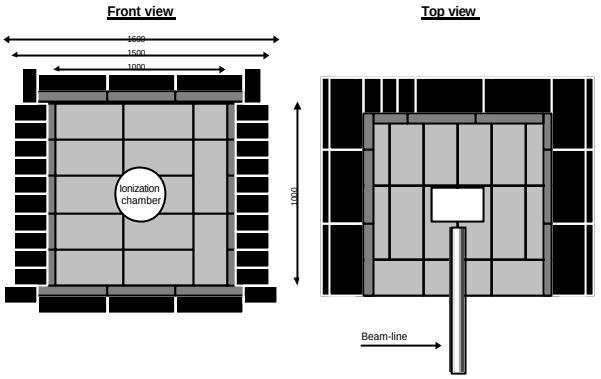

Fig. 4 Schematic view of the radiation shielding.

A twin Frisch-gridded ionization chamber (IC) was used as fission fragment detector. A schematic view of the experimental set-up is shown in Fig. 3. Details about the chamber and associated electronics can be found in Refs. [9, 10] and references therein. With this chamber configuration an efficient particle discrimination is possible. The sample to be measured and a reference ^{237}Np-sample were placed in a back-to-back geometry on the common cathode plate of the IC. In this way, the measured cross sections could be determined relative to the well-known ^{237}Np (n, f) cross section (taken from Ref. [7]). As counting gas P-10 (90%Ar+10%CH_4) was used, kept at a slight over-pressure and refreshed with a constant flow of about 0.1 l/min. The detector was placed at the end of the accelerator beam-line, which resulted in a sample distance of about 8 cm from the neutron producing target. Beam currents of up to 50 μA were used in the experiment, which made it necessary to construct a heavy shielding (shown in Fig. 4) to keep the environmental dose rate below legal limits. Neutrons were effectively thermalized by an outer layer of paraffin, and an inner layer of boron carbide (B_4C) captured away the re-scattered thermal and epithermal neutrons.

Three subsequent campaigns with three freshly prepared ^{233}Pa-targets were performed, each lasting for about 40 days. The individual ^{233}Pa measurements were carried out in runs between 10 h and 24 h each.

3. Data analysis

The first step in the data analysis for each experimental run is to identify the fission events by sorting out the background stemming from other events. With the high β^- activity of the ^{233}Pa samples (activity in the range from about 0.5 to 1 GBq) an effective background subtraction was necessary. This could be achieved by making use of the information obtained both from the

anode and grid of the IC. The center-of-gravity information of the ionization track, contained in the grid signal, was determined and plotted versus the pulse height of the fission fragments (see Fig. 5). In this representation a clean separation between fission fragment pulses and pile-up pulses could be achieved. The corresponding fission fragment pulse height distribution for both the ^{237}Np and ^{233}Pa after background subtraction is shown in Fig. 6 for E_n = 2.0 MeV.

Another important issue to be tackled was the decay of ^{233}Pa into ^{233}U. This resulted in an increasing fraction of the registered fission events from the ^{233}Pa target actually stemming from fission of ^{233}U. Unfortunately, the differences of the fission cross-section for ^{233}U given in the available data libraries were not negligible, which made additional measurements of this cross-section necessary, maintaining exactly the same geometry. Since the shielding is actually influencing the neutron spectrum, the ^{233}U fission cross-section measurements were actually performed both with and without the shielding in place.

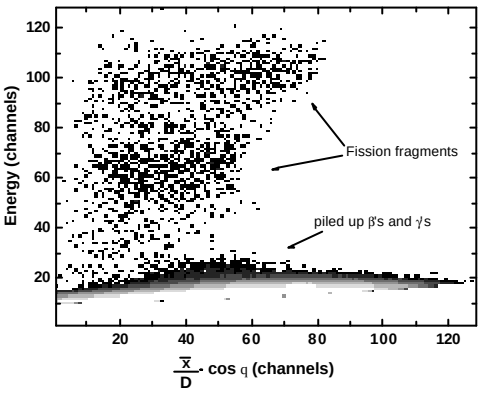

Fig. 5 Plot of the pulse height distribution versus the particle range. This two-dimensional distribution was used to identify the fission fragments.

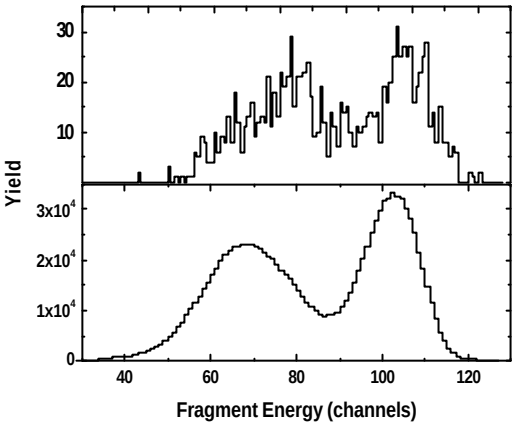

Fig. 6 Fission fragment pulse height distribution for ^{233}Pa (top) and ^{237}Np (bottom) after background rejection for E_n = 2.0 MeV.

4. Statistical calculations

Based on the experimental results presented in this work, a new calculation of the ^{233}Pa(n,f) cross-section was performed, too. Backed up by the successful fission cross-section evaluations for ^{235}U and ^{237}Np (see Refs. [11, 12] and references therein) a new self-consistent neutron cross-section evaluation for ^{233}Pa in the neutron incident energy range up to the second chance fission threshold has been performed. The fission cross-section for n+^{233}Pa was calculated up to 20 MeVin competition with all other possible processes [13, 14]. We take into account that, in the studied incident neutron energy range, the neutron interaction takes place through both direct and compound nucleus mechanisms.

The total cross-section, the direct scattering cross-sections and the neutron transmission coefficients were provided by coupled channel calculations performed with the ECIS95 code [15], using the phenomenological deformed optical model potential parametrization for the actinide region given in Ref. [16]. The compound nucleus mechanism was treated in the

framework of the statistical model for nuclear reactions. For the residual nucleus a discrete level spectrum up to 306.05 keV was assumed consisting of 22 discrete levels adopted from the Reference Input Parameter Library (RIPL) [17]. The continuum level spectrum was described by the composite level density function of Gilbert and Cameron [18].

Due to the lack of experimental data for the neutron s-wave average level spacing at the neutron binding energy B_n for ^{233}Pa, the level density parameter *a* was obtained theoretically by using the Gilbert and Cameron [18] recipe.

The fission cross-section was calculated with the STATIS code [11, 12, 19]. In this code every transitional state is represented by a double-humped fission barrier. Each fission barrier is constructed from inverted parabolas for the inner and outer barrier and a parabolic barrier for the isomeric well. A schematic view of the double-humped fission barrier and the possible decay mechanisms is given in Fig. 7.

The transmission coefficients for absorption and direct fission are calculated in the Jeffreys-Wentzel-Kramer-Brillouin approximation using the optical model for fission. The direct, indirect, and isomeric fission processes are taken into account as well as sub-barrier effects. For the transition states both the discrete and continuum part of the spectrum is considered.

For the compound nucleus ^{234}Pa the discrete transitional band-head states were considered to be the same as for ^{238}Np [12], and the rotational bands were built on them. The continuum part of the transition state spectrum was again calculated with the Gilbert and Cameron level density composite formula. An additional collective enhancement factor, specific to the nuclear shape symmetries at each saddle point, was taken into account. The compound nuclei ^{232,233,234}Pa were considered to exhibit mass symmetry and axial symmetry at the inner barrier A, and mass asymmetry and axial symmetry at the outer barrier B.

The parameters of the fundamental double-humped fission barrier for the compound nucleus ^{234}Pa were chosen in such a way that the best agreement between the calculations and the directly measured experimental data [9,10] was achieved. More information concerning the higher fission chances and the calculation of the reaction cross-sections for the ^{232,233}Pa compound nuclei can be found in Ref. [14].

The selected fission barrier parameters were V_A = 6.05 MeV, $\hbar w_A$ = 0.65 MeV, V_B = 6.52 MeV, $\hbar w_B$ = 0.45 MeV, V_I = 2.50 MeV, and $\hbar w_I$ = 1.00 MeV, where A denotes the inner fission barrier, B the outer one, and I the isomeric well.

The most important parameters are the outer and inner barrier heights. The former defines the threshold energy, the latter is very important for the absolute value of the fission cross section. For example a change of 10% in the inner barrier height would change the absolute value of the fission cross-section by 40%. The mentioned numerical values have been chosen to be compatible with the directly measured experimental data. The resonance structure only appears if the isomeric well has a certain depth, as given above.

The result of the calculation for the ^{233}Pa(n,γ) cross-section up to 20 MeV is presented in Fig. 8 and for the fission cross-section up to 10 MeV is included in Fig. 10 [14].

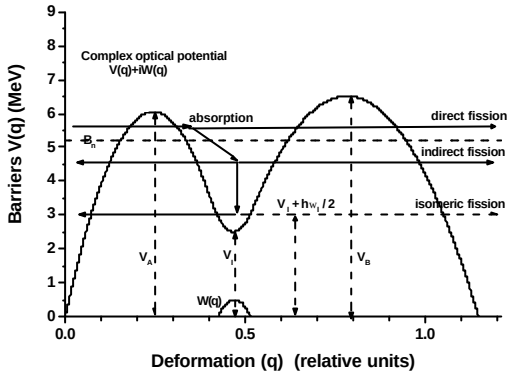

Fig. 7 Schematic view of the double humped fission barrier with all the possible decay mechanism involved.

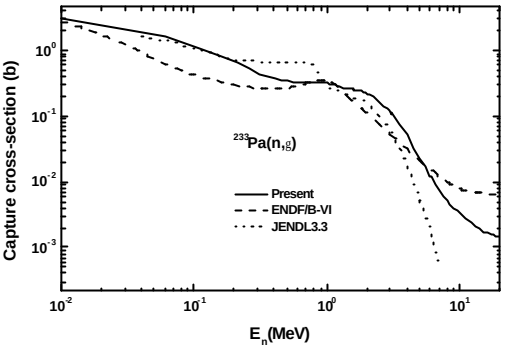

Fig. 8 Present calculations (full line) of the capture cross-section for ^{233}Pa(n,γ) in comparison with evaluated libraries.

5. Results and discussion

After all corrections have been applied and the fission events clearly identified, the cross-section of ^{233}Pa (σ_{Pa}) relative to the cross-section of ^{237}Np (σ_{Np}) can be calculated according to

$$s_{Pa} = \frac{N_{Np} \cdot C_{Pa+U}}{N_0 \cdot e^{-l \cdot t} \cdot C_{Np}} \cdot s_{Np} - \left(e^{-l \cdot t} - 1\right) \cdot s_U \,, (1)$$

where N_{Np}, N_0, are the number of nuclei in the ^{237}Np reference sample and the ^{233}Pa sample at the time of production. C_{Pa+U} and C_{Np} are the measured number of fission events. C_{Pa+U} is actually the sum of the fission events from ^{233}Pa and ^{233}U, which can be expressed as $C_{Pa+U} = C_{Pa} + C_U$. Since the fission cross-section of ^{233}U, as already mentioned before has a too large spread in the available evaluated data files, this quantity has also been measured both with and without shielding. The resulting cross-section values are shown in Fig. 9. As it is obvious from this figure the values with shielding deviate strongly at the lower and higher neutron energies from the values measured without shielding. This has been understood and is due to scattering of neutrons on the shielding material yielding a low-energy tail in the neutron spectrum for neutron energies below 3 MeV. The effect was quantified by simulations with the Monte Carlo transport code MCNP [20]. Since ^{233}Pa(n,f) and ^{237}Np(n,f) are both threshold reactions, the influence of the low energy neutron tail is negligible, however for the fissile ^{233}U-isotope a significant effect was observed (cf. Fig. 9). At the higher neutron energies (above 6 MeV) also higher fission cross-section values for ^{233}U(n,f) have been observed using the shielding. Here a closer investigation of the neutron spectrum revealed parasitic neutron peaks about 5.4 MeV lower than the main peak. This was finally explained by secondary neutron production reacting on ^{16}O present due to oxidation of the solid TiD. A more detailed explanation can be found in Ref. [10]. After identification of the different sources of parasitic neutrons, finally the fission cross-section for ^{233}Pa could be calculated based on eq. (1). The resulting numerical values are given in Table 1 and in Fig. 10 together with the available evaluations, our new calculation and a recent indirect determination of the ^{233}Pa fission cross-section [21].

As it is obvious from this figure, the directly measured cross-section data are lower than both the evaluations from ENDF/B-VI and JENDL3.3 as well as the indirect measurements of Ref. [21]. Also the threshold energy is deviating from the prediction of JENDL3.3 but is in agreement with the threshold from ENDF/B-VI and Ref. [21]. The indirect determination of the fission cross-section in Ref. [21] is based on fission probability measurements using the ^{232}Th(^{3}He,pf)^{234}Pa transfer reaction. In this way the fission probability of the compound nucleus in neutron induced fission of ^{233}Pa was determined, and the compound nucleus formation cross-section was obtained by model calculations. The ^{233}Pa(n,f) cross-section was then calculated as the product of the experimental fission probability and the theoretical compound nucleus formation cross-section. Since the reliability of such an ansatz is debatable for a particle transfer reaction a deviation from the direct measured fission cross-sections is not surprising. A more elaborated discussion the reader can find in Ref. [14].

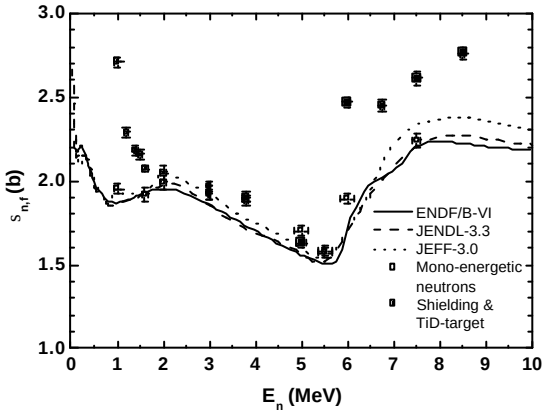

Fig. 9 Results of the ^{233}U fission cross-section measurements, with (open symbols) and without (full symbols) shielding compared to library files (curves).

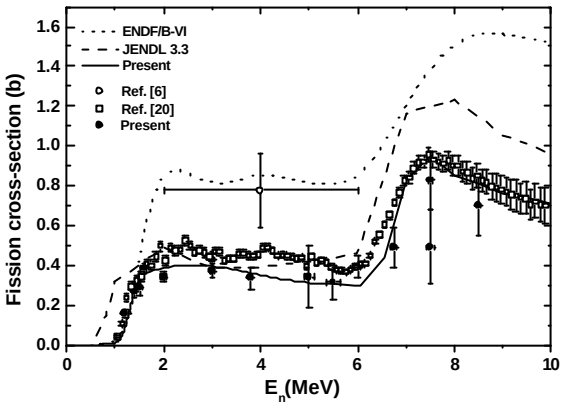

Fig. 10 The measured ^{233}Pa fission cross-section (full points) compared to the recent indirect measurement of Ref. [21], the new calculation (dotted line) [14] and the existing library files (curves).

Table 1 The measured ^{233}Pa fission cross section

E_n (MeV)	σ(b)	E_n (MeV)	σ(b)
1.00 +/- 0.06	-0.021 +/- 0.060	3.80 +/- 0.03	0.336 +/- 0.054
1.20 +/- 0.06	0.155 +/- 0.019	5.00 +/- 0.10	0.342 +/- 0.154
1.40 +/- 0.05	0.268 +/- 0.030	5.50 +/- 0.14	0.312 +/- 0.083
1.50 +/- 0.05	0.288 +/- 0.042	6.00 +/- 0.07	0.390 +/- 0.056
1.60 +/- 0.05	0.384 +/- 0.027	6.75 +/- 0.06	0.490 +/- 0.098
2.00 +/- 0.04	0.342 +/- 0.023	7.50 +/- 0.05	0.827 +/- 0.146
3.00 +/- 0.04	0.371 +/- 0.036	7.50 +/- 0.08	0.490 +/- 0.187
3.00 +/- 0.04	0.426 +/- 0.040	8.50 +/- 0.04	0.699 +/- 0.149

If we consider now the new calculations of the ^{233}Pa(n,f) cross-section [14] as already

discussed in chapter 4, the agreement with the experimental results is very close (see Fig. 10).

One should also mention the very recent calculation of the fission cross-section of ^{233}Pa [22] based on our first experimental data [9]. Probably due to the limited data set the calculations of Ref. [22] show less agreement with the experimental data as the one described in chapter 4.

6. Conclusion

The fission cross-section of ^{233}Pa has been determined with mono-energetic neutrons in the energy range E_n = 1.0 to 8.5 MeV with sufficient accuracy for technical application. In addition, a theoretical calculation of the reaction cross-sections has been performed using the STATIS code, resulting in a good description of the experimental data. The direct measurement and the self-consistent modeling of the cross-section have shown that the indirect determination of the cross-section [21] is too high due to the questionable validity of the ansatz on which those data are based.

References

1) K. Furukawa, Y. Kato, et al., Proc. of Japan-US Seminar on Thorium Fuelled Reactors, Oct. 1982, Naora, Japan.
2) C. D. Bowman, E. D. Arthur, et al., Nucl. Instr. and Meth. **A 320,** 336 (1992).
3) F. Carminati, R. Kapisch, et al., CERN/AT/93-47(ET) (1993).
4) V.G. Pronyaev, INDC(NDS)-408 (1999).
5) C. Rubbia, J.A. Rubio, S. Buono, et al., CERN/AT/95-44(ET) (1995).
6) H. R. von Gunten, R. F. Buchanan, A. Wyttenbach, et al., Nucl. Sci. and Eng. **27**, 85 (1967).
7) Cross Section Evaluation Working Group, edited by P. F. Rose, BNL-NCS-17541 (ENDF-201), (1991).
8) K. Shibata, T. Kawano, et al., J. Nucl. Sci. Technol. **39**, 1125 (2002).
9) F. Tovesson, F.-J. Hambsch, A. Oberstedt, et al., Phys. Rev. Lett. **88**, 062502-1 (2002).
10) F. Tovesson, F.-J. Hambsch, A. Oberstedt, et al., Nucl. Phys. **A733**, 3 (2004).
11) G. Vladuca, A. Tudora, F.-J. Hambsch, et al., Nucl. Phys. **A720**, 274 (2003).
12) G. Vladuca, A. Tudora, F.-J. Hambsch, S. Oberstedt , Nucl. Phys. **A707**, 32 (2002).
13) G. Vladuca, F.-J. Hambsch, A. Tudora, et al., Phys. Rev. **C69,** 0216xx(R) (2004).
14) G. Vladuca, F.-J. Hambsch, A. Tudora, et al., submitted to Nucl. Phys. A.
15) J. Raynal, 1994, Notes on ECIS94, CEA-N-2772 and private communication.
16) G. Vladuca, A. Tudora, M. Sin, Rom. J. Phys. 41, 515 (1996) and Reference Input Parameter Library (RIPL), Segment IV, id 600.
17) RIPL, Segment II, Discrete Level Schemes, recommended file.
18) A. Gilbert, A. G. W. Cameron, Can. J. Phys. **43**, 1446 (1965).
19) G. Vladuca, M. Sin, in: Proceedings of the International Conference on Nuclear Data for Science and Technology, May 19-24, 1997, Trieste, Bologna, Italy, p. 976.
20) J. F. Briesmeister (ed.), LA-13709-M, 2000.
21) M. Petit, Thesis, University of Bordeaux-I, 2002; G. Barreau et al., private communication.
22) J. Mesa, J.D.T. Arruda-Neto et al., Phys. Rev. **C68**, 054608 (2003).